Emulating isomerization with two-dimensional Coulomb crystals

Naoto Mizukami [1,2,3,*] Gabriele Gatta [2,4] Lucia Duca [1,2] and Carlo Sias [1,2,5,†]

[1] *Istituto Nazionale di Ricerca Metrologica (INRIM), 10135 Torino, Italy*

[2] *European Laboratory for Nonlinear Spectroscopy (LENS), 50019 Sesto Fiorentino, Italy*

[3] *Politecnico di Torino, 10129 Torino, Italy*

[4] *Department of Physics and Astronomy, University of Florence, 50019 Sesto Fiorentino, Italy*

[5] *Istituto Nazionale di Ottica, Consiglio Nazionale delle Ricerche (CNR-INO), 50125 Firenze, Italy*

(Received 13 October 2025; revised 24 December 2025; accepted 18 August 2026; published 30 October 2026)

Isomerization is a fundamental process in chemistry. We use a two-dimensional Coulomb crystal to emulate molecular isomerization and characterize its physical mechanisms. In our molecular analog, the externally controlled confining potential determines the crystal's potential energy surface (PES), thereby playing the role that the molecular electronic state plays in determining the PES in a molecule. We focus on a crystal of six $^{138}Ba^{+}$ ions exhibiting a region of bistability, and use a Monte Carlo simulation to extract the PES as a function of the trap aspect ratio. Experimentally, we prepare the ions in a stable isomer, quench the PES to populate a metastable isomer and use a configuration-resolved imaging to detect isomerization in real time. We measure isomers' populations in the bistability region and compare them with a theoretical model to extract the crystal's temperature. Moreover, we derive the transition rates from the measured transient times, thus providing a full characterization of the isomerization process. Our work sets a platform for emulating molecular processes, paving the way to study quantum superpositions of crystal configurations and control isomeric excitations in two-dimensional Coulomb crystals.

DOI: 10.1103/bpjf-p1yk

I. INTRODUCTION

Atomic systems have been used successfully over the past few decades for simulating a wide range of physical phenomena. This progress is largely due to the exceptional degree of control over key parameters that govern the particles' dynamics, such as their confinement and interactions. Both neutral atoms and trapped ions have been used to emulate physical models, e.g., of condensed matter [1,2], high-energy physics [3], and astrophysics [4,5], by replicating the corresponding Hamiltonians. This success stems not only from the precise control of particle dynamics, but also from the fact that the characteristic timescales in atomic systems can be made much more accessible than for other physical systems, e.g., electrons in a solid. For instance, Bloch oscillations, a phenomenon occurring at a picosecond timescale for electrons in a superlattice [6], lie in the millisecond range for atoms in an optical lattice [7].

Trapped ions, when cooled to sufficiently low temperatures, form Coulomb crystals: ordered structures shaped by mutual repulsion and external confinement [8]. These structures resemble molecular configurations: The ions provide the analog of nuclei, while the externally imposed trapping potential, together with the Coulomb repulsion, determines the crystal's potential energy surface (PES), thus playing the role that the molecular electronic state plays in determining the PES of a molecule [9]. This analogy is particularly striking in two-dimensional (2D) crystals. For example, five or six ions in a symmetric two-dimensional potential can arrange themselves in a geometry that is reminiscent of an aromatic ring in a molecule, like in pyrrole or benzene [10]. Similarly to a molecule, a two-dimensional crystal of ions has an energy spectrum characterized by a vibrational and a rotational quantum number [11]. However, the size of an ion crystal is approximately 5 orders of magnitude larger than that of a benzene molecule, resulting in an energy spectrum that is much shallower. As a result, the internal dynamics of the crystal occurs on far more accessible timescales with respect to the ones of a molecule for its real-time observation.

Like molecules, two-dimensional ion crystals can exhibit isomerization, i.e., changes in the spatial arrangement of the particles that are triggered by variations in the confining potential [12,13]. Planar two-dimensional ion crystals provide a well-established framework for investigating structural phase transitions [14–17]. A notable example is the linear to zigzag transition [18], which was investigated in different contexts, e.g., to study its second-order phase transitions nature [19], and to investigate the formation of topological defects [20]. Moreover, there can be conditions in which multiple configurations are stable. An example is a quasi-2D crystal, in which

*Contact author: mizukami@lens.unifi.it

†Contact author: c.sias@inrim.it

Published by the American Physical Society under the terms of the Creative Commons Attribution 4.0 International license. Further distribution of this work must maintain attribution to the author(s) and the published article's title, journal citation, and DOI.

the particles can be either in a zigzag or a zagzig configuration, both having the same energy. This physical system was suggested for creating quantum superposition between crystal configurations [21].

In real molecules, isomerization occurs when the molecule rearranges on a different minimum of the PES, with a process that can be triggered in different ways, e.g., via thermal excitation or quantum tunneling [22]. The PES can be modified by multiple mechanisms, e.g., via laser-driven population of electronically excited states [23,24], the use of mechanical stress [25], the application of electric fields [26], or the use of different solvents [27]. In Coulomb crystals, isomerization can be triggered by changing the external confinement [28,29], by quantum tunneling [30], or by locally exciting one ion in the crystal to a Rydberg state [31]. In particular, the number of different stable isomers increases with the number of particles [32,33], and the presence of several stable crystal configurations was observed for a number of ions approaching 100 [34].

In our work, we use a two-dimensional Coulomb crystal to emulate the process of isomerization in a molecule. Isomerization is triggered by a change of the PES, which is realized by controlling the aspect ratio of the 2D harmonic trapping potential [13]. To do so, we tune the dc voltage applied to the end caps of our Paul trap [35], practically applying a static deconfining potential across the y axis and a confining potential along the x and z axes. This potential adds on the confining pseudopotential created by the rf fields in the x-y plane. As a result, the crystal lays in the y-z plane, and as the dc voltage changes, the trap aspect ratio $\alpha = \omega_y/\omega_z$ changes [10], where ω_z and ω_y are the trap frequencies along the two axes of the confinement plane. As a result, it is possible to quench the aspect ratio and observe in real time the dynamics of the crystal while undergoing isomerization [36]. This property makes it possible to investigate bistability regions, in which more than one isomer is populated, with the particles moving between one isomer to the other triggered by thermal fluctuations.

II. PHYSICAL MODEL AND ESTIMATION OF THE POTENTIAL ENERGY SURFACE

In our study, we focus on the specific case of six $^{138}Ba^{+}$ ions forming a two-dimensional Coulomb crystal. We identify a range of parameters in which the crystal undergoes isomerization by passing from a structure formed by six ions in a benzenelike ring to a crystal formed by five ions in a ring and one ion at the center of the trap [see insets in Fig. 1(b)]. We will refer to these configurations as "hexagon" and "pentagon" isomers, respectively. This specific example has the advantage that isomerization is controlled by the displacement of one of the ions in the crystal from the center of the trap to the outer ring. As a result, this displacement can be used as the only parameter characterizing the PES.

In order to identify the values of α at which isomerization occurs and extract the corresponding PES, we use a Monte Carlo simulation to search for the lowest-energy configuration [37,38]. In the simulation (see Appendixes), the equilibrium position of six ions in the trap is found by an iterative process. In each step of this process, two random particles are moved around their initial position and displaced to the position corresponding to the lowest energy. In an initial set of simulations, we extracted the ions' equilibrium positions and their total potential energy (confinement and electrostatic energies) as a function of the aspect ratio α. This was done by gradually increasing α, using the equilibrium configuration from the previous step as the starting point for each new simulation. As α increases, isomerization occurs at a threshold value, corresponding to an abrupt switching of the ions' equilibrium position from the pentagon to the hexagon isomer. After reaching the upper limit of α, we reversed the process and gradually decreased α. Notably, the results revealed pronounced hysteresis, with the isomerization threshold and equilibrium energies depending on the direction of the sweep. This behavior signals the presence of bistability between the two distinct isomers. Figure 1(b) summarizes the results of this simulation by plotting the potential energies V_{pen} and V_{hex} at equilibrium for the pentagon and hexagon isomers, respectively. For $\alpha \lesssim 1.19$, the lowest energy configuration corresponds to the pentagon isomer (orange), while for $\alpha \gtrsim 1.19$, the lowest energy configuration is the hexagon isomer (purple). Interestingly, for $1.13 \lesssim \alpha \lesssim 1.23$ both isomers can be prepared as a stable solution of the Monte Carlo simulation, a clear signature of bistability. Crucially, the scale of the energy difference between the two isomers lies in the tens of millikelvin range, i.e., values that can be explored with typical trapped ion kinetic energies.

To extract the PES along the isomerization path, we ran a second set of Monte Carlo simulations. In this set, we forced one ion to stay at a specific distance r_{fix} from the center of the trap [see insets in Fig. 1(c)]. As r_{fix} is varied, the minimum-energy path (MEP) on the PES is reconstructed from the minimum-energy crystal configuration obtained for each value of r_{fix}. Figure 1(c) plots the energy of six ions obtained with the Monte Carlo simulation as a function of r_{fix} for $\alpha = 1.20$, corresponding to $(\omega_z, \omega_y)/(2\pi) = (100, 120)$ kHz. The energy along the minimum-energy path shows a double-well behavior, typical to the PES in the presence of bistability. Crucially, we observe that the double well is formed in the bistable region, and the energy offset between the two wells can be continuously changed by varying α [see Fig. 1(a)]. For each value of α, we extract the height of the energy barrier between the pentagon (hexagon) and the hexagon (pentagon) isomers V_{p2h} (V_{h2p}) as the difference between the energy minimum of the well and the energy V_{sad} at the saddle point: $V_{\mathrm{p2h}} = V_{\mathrm{sad}} - V_{\mathrm{pen}}$ ($V_{\mathrm{h2p}} = V_{\mathrm{sad}} - V_{\mathrm{hex}}$). We observe the presence of a double well in the PES in the similar region of α in which we observe hysteresis in the first set of simulations. In the symmetric case for which $V_{\mathrm{p2h}} = V_{\mathrm{h2p}}$, we find a barrier height on the order of 7.9 mK and a distance between the two minima of approximately 9.6 μm. For these parameters, tunneling through the barrier is negligible, and the observed dynamics is purely classical.

III. EXPERIMENTAL IMPLEMENTATION AND RESULTS

Experimentally, we exploit the hysteresis shown in the Monte Carlo simulation to configure ions into a metastable isomer. Figure 2(b) shows a typical experimental run. The ions are first prepared in a pentagon isomer by setting α to

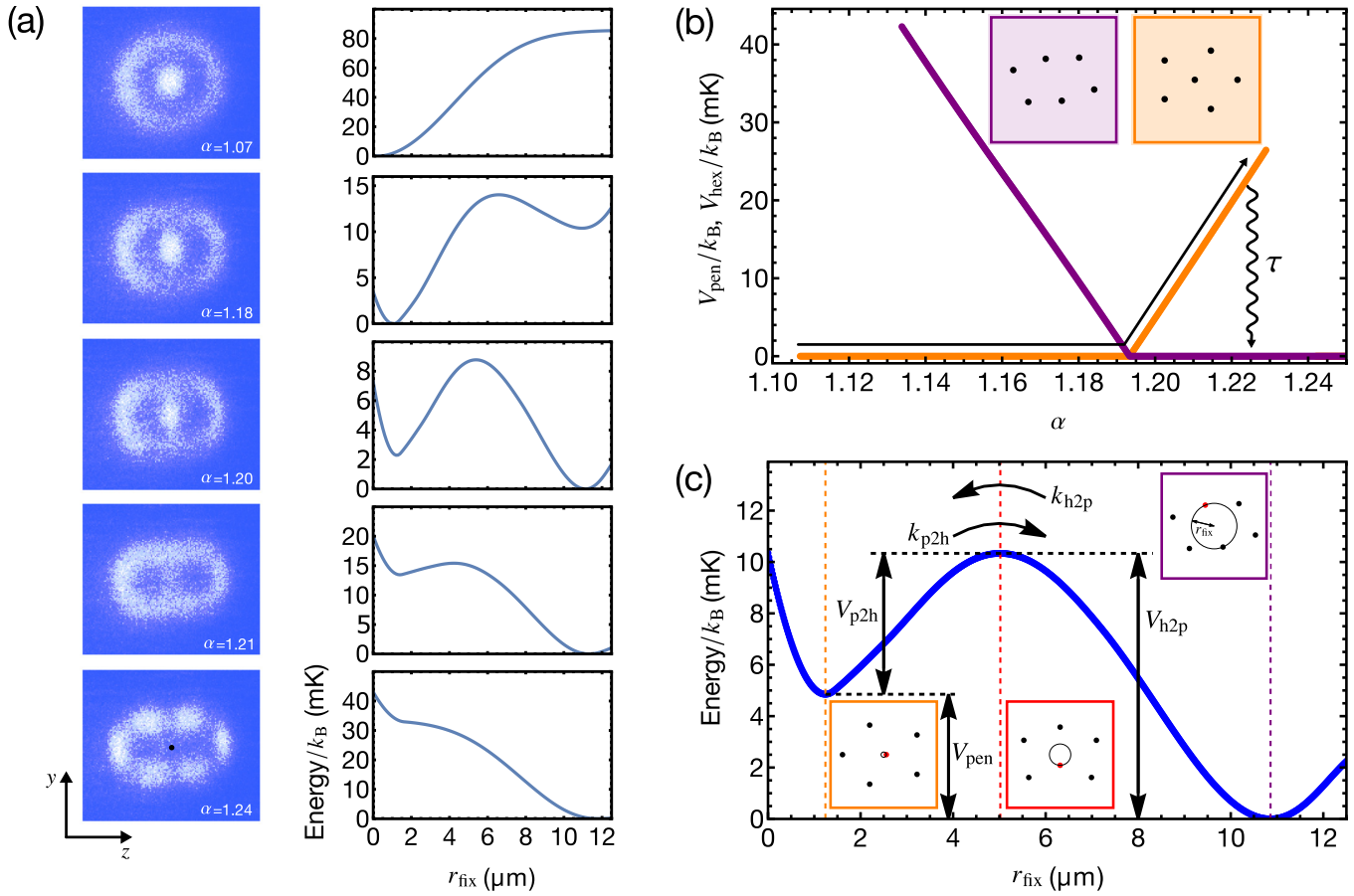


FIG. 1. Isomerization and bistability in a two-dimensional crystal formed by six ions. (a) Left panels: Experimental images of six ions across the bistable range as a function of the trap aspect ratio α. The images are taken with 1 s exposure time. We note that the crystal undergoes orientational melting for the lowest values of α. The point in the lowest image indicates the coordinates zero. Right panels: Corresponding potential energy surfaces of the crystal as extracted from a Monte Carlo simulation. (b) Potential energies of the pentagon (orange) and hexagon (purple) isomers as a function of α. By quenching α, it is possible to populate a metastable isomer (black arrow), which then decays by thermal fluctuations to the lowest-energy one (wavy arrow). (c) Energy along the minimum-energy path on the potential energy surface for $\alpha = 1.20$. The minimum-energy is extracted by forcing one ion to stay at a distance $r_{\rm fix}$ from the trap center (see insets) in the Monte Carlo simulation. The calculated energies for the two minima and the saddle point make it possible to extract the barrier heights $V_{\rm p2h}$, $V_{\rm h2p}$ and the transition rates $k_{\rm p2h}$, $k_{\rm h2p}$. In the plots, an energy offset is subtracted to set the lowest energy to zero.

a value $\alpha_1 = 1.11$ at which no metastable configuration is present. After 10 ms of laser cooling, α is rapidly quenched to a value α_2 in less than 50 μs, a timescale that is limited by the voltage supply bandwidth. For $1.13 \lesssim \alpha_2 \lesssim 1.23$, the crystal experiences bistability between the hexagon and the pentagon isomers. The crystal is kept at $\alpha = \alpha_2$ for 20 ms before it is changed back to α_1 and a new cycle can begin. Laser cooling remains on for the whole cycle, and we can assume the ions to be at the same temperature at equilibrium. The excess micromotion is compensated for. Moreover, in our trap geometry the rf electric field is predominantly orthogonal to the plane of the crystal [35], and the residual excess micromotion of the ions laying out of the trap axis has only a small projection onto the y-z plane, where the isomerization dynamics takes place (see Appendixes).

To distinguish between the two configurations, we have implemented a setup to detect fluorescence from only the center region of the trap [see Fig. 2(a) and Appendixes]. We identify what isomer is formed by the ions by measuring the photon counting rate n. Since the pentagon isomer is characterized by one ion in the trap central region, the corresponding photon rate $n_{\rm pen}$ is larger than the photon rate $n_{\rm hex}$ measured in the case of a hexagon isomer. Whenever bistability occurs, the crystal continuously jumps from one isomer to the other because of thermal fluctuations. Density distribution of ions in a crystal across the bistable condition is exhibited in the images in Fig. 1(a) taken with the exposure time of 1 s. Within the bistable region, we observe a photon rate $n_{\rm bis}$ that lies between the two limiting cases, i.e., $n_{\rm hex} \leqslant n_{\rm bis} \leqslant n_{\rm pen}$. Immediately after the quench, the crystal remains in the metastable configuration; the configuration probability then relaxes toward equilibrium. During each experimental sequence, the photon arrival times are recorded relative to the start of the sequence. Submillisecond time resolution is achieved by accumulating data over repeated quenches and binning the photon arrival times in 0.1 ms intervals. Figure 2(c) shows the average photon rate detected for multiple experimental runs. After the quench in the aspect ratio, we observe an exponential decay

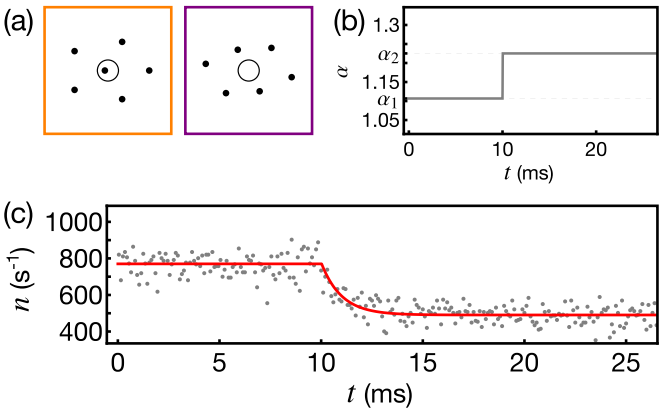


FIG. 2. Real-time observation of isomerization. (a) Monte Carlo generated equilibrium position of the ions in the pentagon and hexagon isomers. A configuration-resolved imaging is set by observing the fluorescence only from the center of the trap (black circle). (b) Typical experimental run. The trap aspect ratio α is quenched from $\alpha_1 = 1.107$ to the variable value α_2 at $t = 10$ ms. (c) Photon rate of the fluorescence observed in 2072 sequences for $\alpha_2 = 1.225$. The fluorescence detected from the central ion [circle in panel (a)] decreases exponentially after quenching ($t > 10$ ms), witnessing the relaxation from the initial pentagon isomer to a bistable regime.

of the photon rate to $n_{\rm bis}$, a signature of the occurrence of isomerization.

In the bistability region, it is possible to define a probability $p_{\rm hex}$ ($p_{\rm pen}$) for the crystal to be in the hexagon (pentagon) isomer at a given time. These probabilities can be estimated with the photon rate, since its value integrated over time is the result of contributions from the time the crystals spend in each isomer, $n_{\rm bis} = p_{\rm hex} n_{\rm hex} + p_{\rm pen} n_{\rm pen}$. As a result, the probabilities associated with each isomer read

$$p_{\rm hex} = \frac{n_{\rm pen} - n_{\rm bis}}{n_{\rm pen} - n_{\rm hex}},$$
$$p_{\rm pen} = \frac{n_{\rm bis} - n_{\rm hex}}{n_{\rm pen} - n_{\rm hex}}. \quad (1)$$

Figure 3 shows the probabilities $p_{\rm hex}$ and $p_{\rm pen}$ as a function of α. In the bistable regime, the probabilities $p_{\rm hex}$ and $p_{\rm pen}$ are related to the transition rates by the relation [39]

$$\frac{p_{\rm pen}}{p_{\rm hex}} = \frac{k_{\rm h2p}}{k_{\rm p2h}}, \quad (2)$$

where $k_{\rm h2p}$ ($k_{\rm p2h}$) is the transition rate for the crystal changing from the hexagon (pentagon) to the pentagon (hexagon) isomer [see Fig. 1(b)]. Following Arrhenius equation, the transition rates are related to the temperature T via the relation $k_{\rm h2p(p2h)} \propto \exp(-V_{\rm h2p(p2h)}/k_{\rm B}T)$ [40], where $k_{\rm B}$ is the Boltzmann constant. Therefore, we can use Eq. (2) to derive the probabilities $p_{\rm hex}$, $p_{\rm pen}$ as a function of the barrier height and the temperature:

$$p_{\rm hex} = \frac{1}{1 + \exp[(V_{\rm p2h} - V_{\rm h2p})/(k_{\rm B}T)]},$$
$$p_{\rm pen} = \frac{1}{1 + \exp[(V_{\rm h2p} - V_{\rm p2h})/(k_{\rm B}T)]}. \quad (3)$$

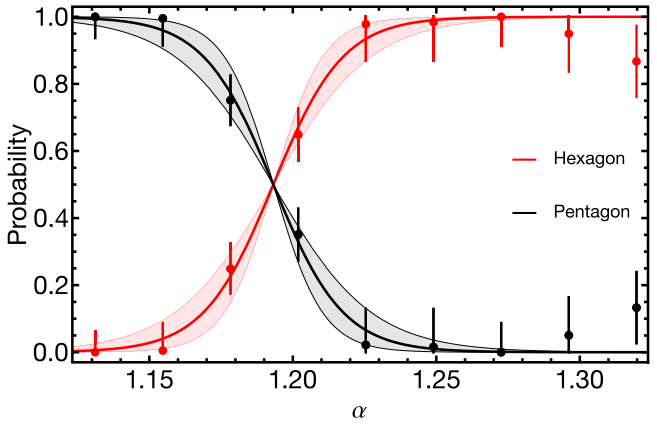


FIG. 3. Bistability of crystal isomers. Probability for a crystal to be arranged in a pentagon (red points) or hexagon (black points) isomer as a function of the trap aspect ratio. The lines are obtained from the simulation data, with the temperature being the only free parameter. The shaded area encloses the functions for which χ^2 is twice as big as the optimal one. The corresponding temperature estimate range is $8.8^{+3.5}_{-2.6}$ mK.

We use Eq. (3) to fit the experimental data in Fig. 3. To this end, we extrapolate the data of $V_{\rm h2p}$ and $V_{\rm p2h}$ from the Monte Carlo simulation, and use the temperature as the only free parameter. We change the temperature in steps of 0.1 mK, and identify the curve that has the lowest χ^2, finding the best-fitting temperature to be 8.8 mK for both $p_{\rm hex}$ and $p_{\rm pen}$ (see solid lines in Fig. 3). To estimate the uncertainty of this temperature estimate, we consider the temperatures for which the χ^2 parameter of the corresponding function is a factor of 2 larger than the best-fitting value. The corresponding

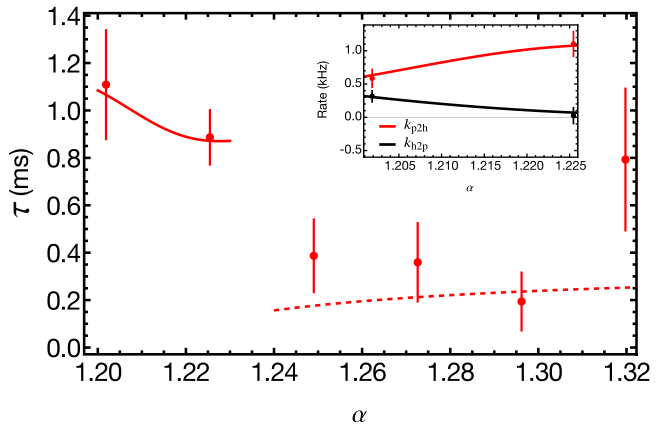


FIG. 4. Isomerization time as a function of the trap aspect ratio. The red points report the isomerization characteristic time τ as a function of α. The times are obtained from an exponential fit of the photon rate data [see Fig. 2(c)]. From the simulation, a double well is predicted for α below approx. 1.23. The solid red line corresponds to the decay expected from a double-well model of isomerization. The dashed line corresponds to the time needed for recooling the crystal below the energy on the potential energy surface corresponding to the edge of the detection region (see text). Inset: Transition rates $k_{\rm h2p}$ (black) and $k_{\rm p2h}$ (red). The corresponding solid lines represent the expected values for the PES extracted in the Monte Carlo simulation.

temperature range is $8.8^{+3.5}_{-2.6}$ mK. This range is shown in Fig. 3 as a shaded area.

We further investigate isomerization by analyzing the transient behavior. By analyzing the data after the aspect ratio quenching, we extract the time constant τ of the decay of the photon rate [see Fig. 2(c)]. Figure 4 shows the scaling of τ as a function of the trap aspect ratio. We observe a faster decay as the aspect ratio is increased. From the Monte Carlo simulation, we can identify two separate regions: For $\alpha \lesssim 1.23$, the system is bistable, as we observe two minima in the corresponding PES, while for $\alpha \gtrsim 1.23$ only the hexagon isomer is stable. In the bistable region, the decay time is related to the rates of the transitions between the two energy minima by the formula $\tau = (k_{\mathrm{p2h}} + k_{\mathrm{h2p}})^{-1}$[39]. By using Eq. (2), we can extract the relation of the rates

$$k_{\mathrm{p2h}} = (\tau(1 + p_{\mathrm{pen}}/p_{\mathrm{hex}}))^{-1},$$
$$k_{\mathrm{h2p}} = (\tau(1 + p_{\mathrm{hex}}/p_{\mathrm{pen}}))^{-1}. \quad (4)$$

We use Eq. (4) and the probabilities p_{hex}, p_{pen} from the data in Fig. 3 to extract the rates from the observed time constant. The results are shown in the inset of Fig. 4, where the solid lines are a fit of the data with the Arrhenius equation. The best-fitting functions of the rates are used to extract the expected behavior for the time constant τ, shown in Fig. 4 as a solid red line. We find an excellent agreement with the experimental data. Out of the bistability region, i.e., for $\alpha \gtrsim 1.23$, we observe a non-negligible decay time that is long compared to the eigenfrequencies of the vibrational modes of the isomers. We attribute this time to be caused by the relatively high kinetic energy acquired by the ions after the quenching, which increases the time required to cool the crystal. From the PES, we can calculate the excess energy the crystal has to lose so that no ion passes by the region of space observed by our imaging system. The dashed line in Fig. 4 shows the time needed by a free particle to lose the excess energy for the cooling light parameters used in the experiment. The curve qualitatively confirms our interpretation.

IV. CONCLUSIONS

In this work, we demonstrate that Coulomb crystals can be used to emulate the physics of isomerization and study the bistabilities that may arise. Thanks to the high level of control on the experimental parameters, we have selectively arranged the crystal in a metastable isomer, thus emulating the physics of isomerization of a molecule. By exploiting the slow dynamics when compared to real molecules and a configuration-resolved detection, we have identified the bistability region and revealed transitions between two isomers that are excited thermally. The potential energy surface of the crystal is obtained using a Monte Carlo simulation and used to derive the barrier heights and the transition rates. Data obtained from the simulation show an excellent agreement with the experimental data and are used to evaluate the temperature of the crystal. Our study paves the way toward exploiting trapped ions for simulations of fundamental mechanism in chemical reactions, e.g., by further modifying the crystal PES by using optical potentials [41] or more complex electric potentials [42]. Moreover, understanding the hysteresis of the isomer formation may play an essential role in the initial state preparation of a quantum computer or a quantum simulator realized with two-dimensional Coulomb crystals [34,43]. Finally, our ability to control the relative height of the wells in the observed double-well potential establishes this system as a versatile platform for studying structural transitions and provides a potential starting point for future extensions toward quantum-coherent regimes. In particular, by lowering the temperature of the crystal either via two-photon cooling [44] or via sympathetic cooling with ultracold atoms [45], or, alternatively, by suitably tailoring the potential energy landscape using, e.g., additional optical potentials, one could envision accessing regimes where quantum tunneling and coherent superpositions of crystal isomers can be achieved.

ACKNOWLEDGMENTS

We thank Stefan Willitsch and Massimo Inguscio for helpful discussions. We also thank Christof Wunderlich for pointing out an error in the first version of the manuscript. This work has been supported by the Project 23FUN03 HIOC, which has received funding from the European Partnership on Metrology, cofinanced from the European Union's Horizon Europe Research and Innovation Programme and by the Participating States. This work was supported by the Cascading Grant Spoke 3 under the PNRR MUR Project No. PE0000023-NQSTI, funded by the European Union—Next Generation EU.

DATA AVAILABILITY

The data that support the findings of this article are openly available [46], embargo periods may apply.

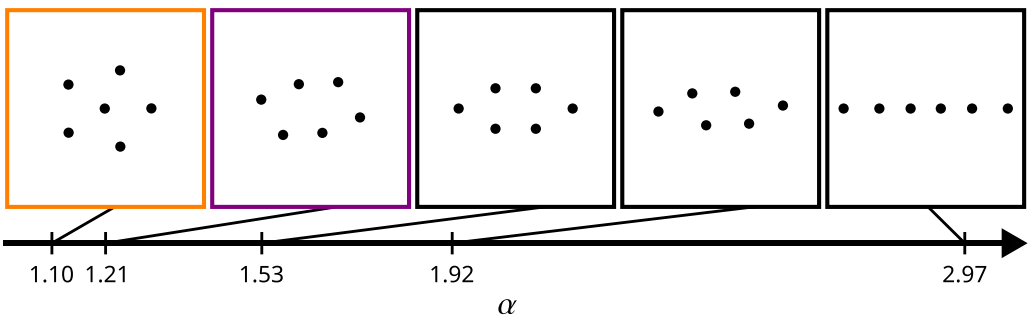


FIG. 5. Configuration of six ions. Configuration of six ions changes from 1D chain, hexagon isomer, and to pentagon isomer depending on the trap aspect ratio α.

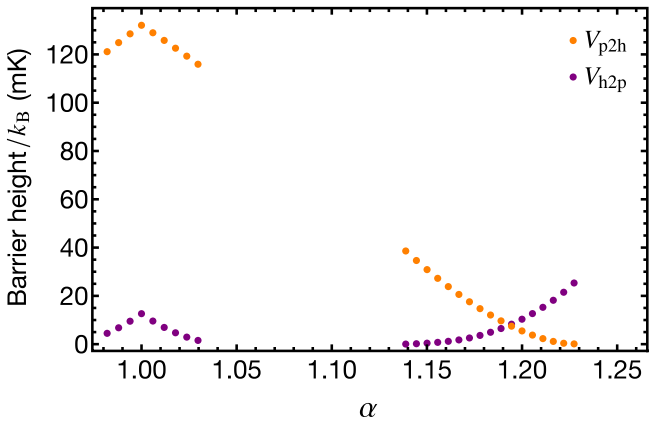


FIG. 6. Barrier heights. Orange (purple) points correspond to a barrier height from pentagon (hexagon) isomer to hexagon (pentagon) isomer.

APPENDIX A: MONTE CARLO SIMULATION

We have conducted Monte Carlo simulations to identify the metastable configuration of the ions and their corresponding potential energy surface. The ions are first placed in a two-dimensional harmonic potential of frequencies (ω_z, ω_y) in a 1 nm grid. The energy E_{tot} of the whole system is given as a sum of the Coulomb energy and the potential energy of the harmonic potential as

$$E_{\text{tot}} = \sum_{n=0}^{6} \frac{1}{2} m\left(\omega_z^2 z_n^2 + \omega_y^2 y_n^2\right) + \frac{1}{2}\frac{e^2}{4\pi\epsilon_0} \sum_{n_1 \neq n_2} \frac{1}{\sqrt{\left(z_{n_1} - z_{n_2}\right)^2 + \left(y_{n_1} - y_{n_2}\right)^2}}, \quad \text{(A1)}$$

where m is the mass of a $^{138}Ba^+$ ion, (z_n, y_n) is the position of nth ion, e is the elementary charge, and ϵ_0 is the dielectric constant of vacuum. Then, the ions' positions are optimized by moving randomly selected two ions at a time within a 10 nm range in the plane. When the positions of the two ions are moved to a new position $(z_{s_1,1}, y_{s_1,1})$ and $(z_{s_2,1}, y_{s_2,1})$ from the original position $(z_{s_1,0}, y_{s_1,0})$ and $(z_{s_2,0}, y_{s_2,0})$, the change in the energy can be expressed as

$$\begin{aligned}
\Delta E_{\text{tot}} = {} & \frac{1}{2} m\left(\omega_z^2\left(z_{s_1,1}^2 - z_{s_1,0}^2\right) + \omega_y^2\left(y_{s_1,1}^2 - y_{s_1,0}^2\right)\right) \\
& + \frac{1}{2} m\left(\omega_z^2\left(z_{s_2,1}^2 - z_{s_2,0}^2\right) + \omega_y^2\left(y_{s_2,1}^2 - y_{s_2,0}^2\right)\right) \\
& + \frac{1}{2}\frac{e^2}{4\pi\epsilon_0} \sum_{n \neq s_1, s_2} \frac{1}{\sqrt{\left(z_{s_1,1} - z_n\right)^2 + \left(y_{s_1,1} - y_n\right)^2}} \\
& + \frac{1}{2}\frac{e^2}{4\pi\epsilon_0} \sum_{n \neq s_1, s_2} \frac{1}{\sqrt{\left(z_{s_2,1} - z_n\right)^2 + \left(y_{s_2,1} - y_n\right)^2}} \\
& + \frac{1}{2}\frac{e^2}{4\pi\epsilon_0} \frac{1}{\sqrt{\left(z_{s_1,1} - z_{s_2,1}\right)^2 + \left(y_{s_1,1} - y_{s_2,1}\right)^2}} \\
& - \frac{1}{2}\frac{e^2}{4\pi\epsilon_0} \sum_{n \neq s_1, s_2} \frac{1}{\sqrt{\left(z_{s_1,0} - z_n\right)^2 + \left(y_{s_1,0} - y_n\right)^2}} \\
& - \frac{1}{2}\frac{e^2}{4\pi\epsilon_0} \sum_{n \neq s_1, s_2} \frac{1}{\sqrt{\left(z_{s_2,0} - z_n\right)^2 + \left(y_{s_2,0} - y_n\right)^2}} \\
& - \frac{1}{2}\frac{e^2}{4\pi\epsilon_0} \frac{1}{\sqrt{\left(z_{s_1,0} - z_{s_2,0}\right)^2 + \left(y_{s_1,0} - y_{s_2,0}\right)^2}}. \quad \text{(A2)}
\end{aligned}$$

ΔE_{tot} is calculated for all points on a grid with a size of 10 and 1 nm spacing around $(z_{s_1,0}, y_{s_1,0}, z_{s_2,0}, y_{s_2,0})$. Then, we update the positions of the two ions to the one that is giving minimum ΔE_{tot}. The procedure is repeated until we get no improvement in the energy after 150 random trials. For each set of parameters, a simulation was repeated for at least 3 times. The crystal configuration of six ions is dependent on the trap aspect ratio $\alpha = \omega_y/\omega_z$. Figure 5 shows configurations of six ions for different values of α found with Monte Carlo simulations. The trap frequencies are varied according to the experimentally determined dependence of the aspect ratio on the dc voltage, which was measured with a parametric heating experiment. To fine-tune the simulated trapping potential to match the experimental one, we calibrated the trap frequencies by comparing the experimental data and the simulation in the condition in which barrier heights between two isomers are balanced. For the Monte Carlo simulation in Fig. 1(b), the simulation becomes less accurate for the metastable isomer around the edges of the bistable region. This is because the PES becomes very flat, and even if there is no minimum in the PES the simulation terminates before converging to a stable solution. To avoid such issues, we assessed the stability of the ion equilibrium positions obtained from Monte Carlo simulations by analyzing the eigenvalues of the Hessian matrix. The presence of a negative eigenvalue indicates that the configuration does not correspond to a true equilibrium. Figure 6 shows barrier heights between stable isomers of a Coulomb crystal of six ions extracted from the Monte Carlo simulation in Fig. 1(c). There exist two regions in α where bistability exists. We choose to investigate the region where the energies of the two configurations cross, around $\alpha = 1.19$.

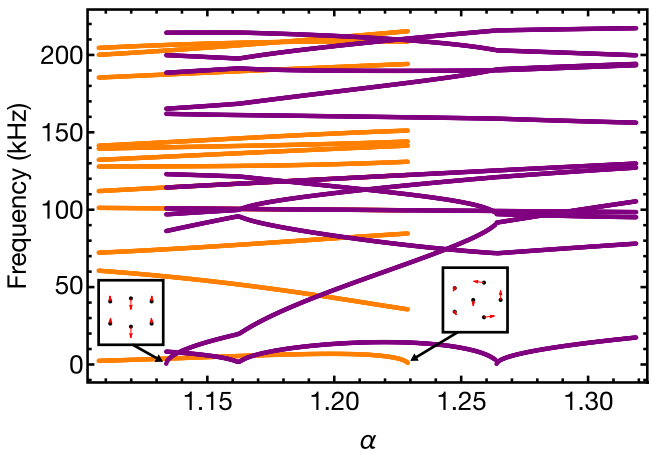


FIG. 7. Eigenfrequencies. Orange (purple) corresponds to eigenfrequencies of a Coulomb crystal in pentagon (hexagon) configuration in 2D.

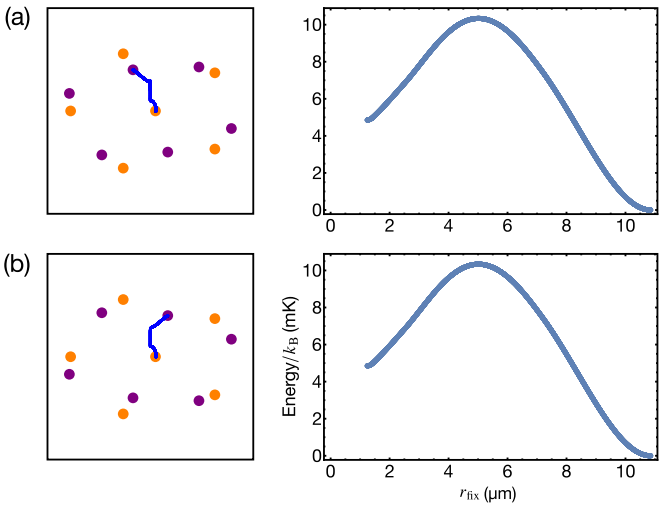


FIG. 8. Minimum-energy paths of one ion from a pentagon configuration to hexagon configuration shown in blue (left panel). Orange (purple) points show the equilibrium positions of ions in a Coulomb crystal in pentagon (hexagon) configuration. Right panel shows the potential energy surfaces associated with the minimum-energy paths in the left panel.

Figure 7 shows the eigenfrequencies calculated for Coulomb crystals of six ions. Eigenfrequencies are calculated by solving Hessian matrix [18].

APPENDIX B: ISOMERIZATION PATH

In two-dimensional plane, there are multiple isomerization paths. Figure 8 shows two MEPs from one pentagon configuration to hexagon configurations for $\alpha = 1.20$. Depending on which path a Coulomb crystal takes during isomerization, six ions are configured in two different hexagon configurations in the mirror symmetry. PES along the two MEPs are identical and the path a Coulomb crystal takes during isomerization would not change its dynamics.

APPENDIX C: PREPARATION AND DETECTION OF TWO-DIMENSIONAL ION CRYSTALS

To confine ions in a two-dimensional plane, our Paul trap has a specific design in which negatively charged dc electrodes are used for axial confinement [10]. By changing the voltages applied to the dc electrodes, the confining potential can vary from one dimension (1D) to 2D. For example, in Fig. 2, the confining potential is quenched from $(\omega_z, \omega_y)/(2\pi) = (98.8, 127.8)$ kHz to $(\omega_z, \omega_y)/(2\pi) = (99.7, 122.1)$ kHz. In the experiment, ions are always laser cooled with two laser beams at 493.5 nm and a repumping laser of 650 nm addressing the $|6s\,^2S_{1/2}\rangle \rightarrow |6p\,^2P_{1/2}\rangle$ and $|5d\,^2D_{5/2}\rangle \rightarrow |6p\,^2P_{1/2}\rangle$ transitions, respectively.

We detect fluorescence at 493.5 nm from the two opposite sides on the axis orthogonal to the trapping plane. On one of the sides, we use two telescopes, each with a magnification of 2, and use a polarizing beam splitter for splitting the signal and send it to a photon counter and a charge-coupled device (CCD) camera. In the first image plane after the first telescope, a pinhole (20 μm diameter) is placed to detect the photons coming from the center region (10 μm diameter) of the trap. The pinhole was aligned by trapping a single ion acting as a reference for the trap center and looking at the picture in the CCD camera. The photon arrival time is recorded with a time-to-digit converter and counted with bins of 0.1 ms. We monitor the number of ions in the trap with a second CCD camera from the opposite side of the plane.

The trap aspect ratio α is changed by varying the dc voltage applied on the end caps V_{dc}. In the quench, we keep $dV_{dc}/dt = 17.9$ V/ms constant, and the overall ramp time is smaller than 50 μs. This time is faster than the characteristic time of the common mode frequencies associated with isomerization (see Fig. 7).

We used the photon correlation technique to detect micromotion and used dc fields to compensate it to $\sim$1.5 V/m on the trap axis. With respect to the excess micromotion in two-dimensional crystals, we note that in our trap design (see Ref. [35]) the axes of the dc quadrupole are rotated by $\pi/4$ with respect to the rf quadrupole in the x-y plane. As a result, the direction of the rf field off the trap axis is orthogonal to the y-z plane where the crystal lays. We have calculated the amplitude of the small projection of the excess micromotion in the y-z plane, and found it $\lesssim$14 nm for the outermost ion in the crystal, corresponding to an energy of $\lesssim$1.2 mK.

APPENDIX D: ORIENTATIONAL MELTING

Depending on the isotropy of the trap potential, Coulomb crystal of six ions may rotate thermally as in an isotropic confinement there is no energetically preferred orientation. This is referred to as an orientational melting resulting in a delocalization of ions in a rotational degrees of freedom [10]. Whether ions exhibit orientational melting is determined by the rotational barrier. Figure 9 shows the rotational barrier for experimental conditions corresponding to the five images in Fig. 1(a). To simulate the rotational barrier, we first determine the equilibrium positions of the ions using a Monte Carlo simulation. Next, we randomly select one ion from the outermost shell of the Coulomb crystal. We then run another simulation starting from its equilibrium position, with the constraint that the selected ion is allowed to move only along a line whose direction is incrementally rotated from the polar angle of the ion's initial position. This simulation is repeated while continuously increasing the angle in steps of $2\pi/1800$, each time using the final position from the previous run as the initial condition for the next. Adjacent minima corresponds to mirror reflective configurations within pentagon or hexagon configurations. It shows that for $\alpha = 1.07, 1.18, 1.20, 1.21$, the height of the rotational barrier is lower than the evaluated temperature of 8.8 K of Coulomb crystals leading to an orientational melting. For $\alpha = 1.24$, maximum height of the rotational barrier is higher than 8.8 mK and thus blocking a crystal from full rotation.

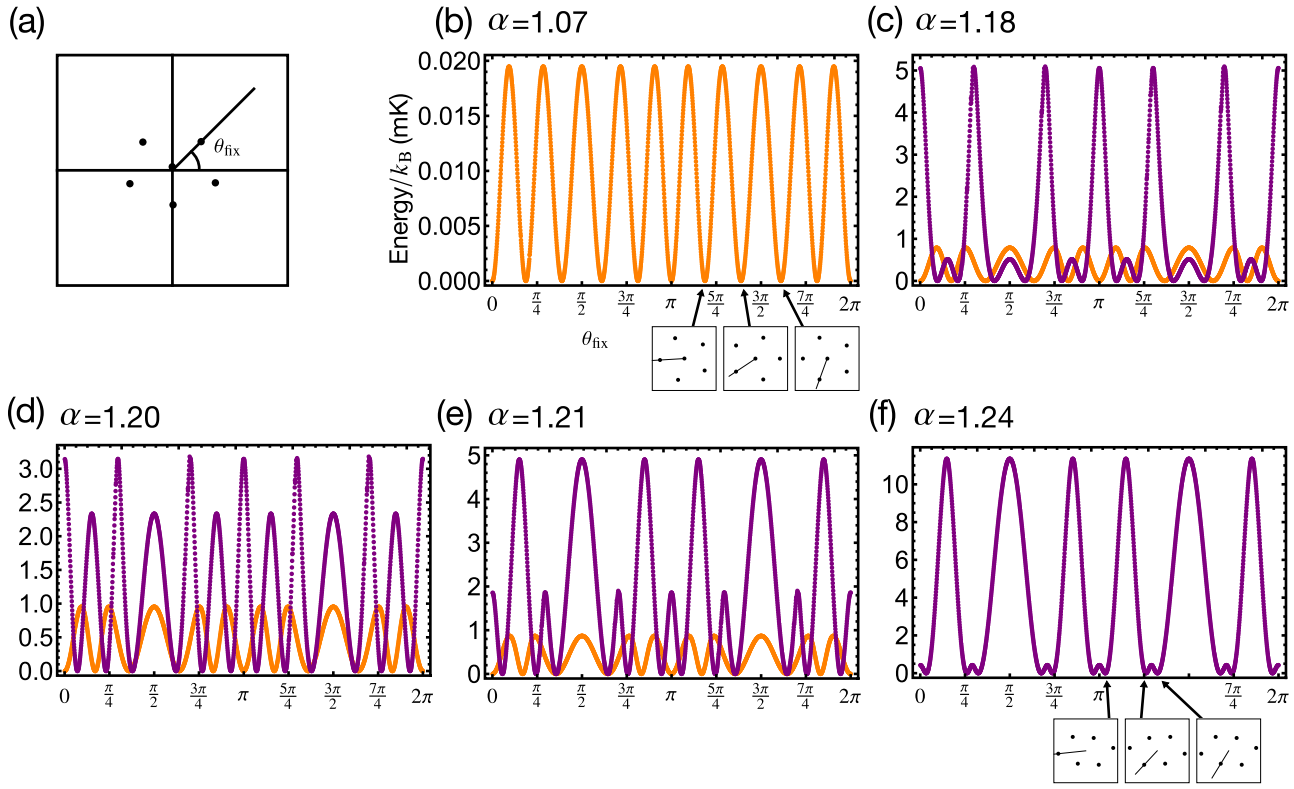


FIG. 9. Rotational barrier. Orange (purple) corresponds to the orientational barrier for pentagon (hexagon) configuration with respect to the equilibrium positions.

APPENDIX E: EXPERIMENTAL PARAMETERS

Here we provide a comprehensive summary of the relevant experimental parameters. Table I reports the rf frequency and amplitude, and the value of the dc voltage used to confine the six-ion crystal. Moreover, relevant imaging system specifications are listed, including magnification, imaging region of interest (ROI), integration time of the photon counts (binning).

TABLE I. Experimental parameters overview. The dc voltage refers to the voltage applied before quenching.

Parameter	Value	Unit
rf frequency	4.446	MHz
rf amplitude (peak to peak)	780	V
dc voltage	−13.4	V
Imaging magnification	2	–
Imaging ROI	25π	μm^2
Binning time	0.1	ms

[1] I. Bloch, J. Dalibard, and S. Nascimbène, Quantum simulations with ultracold quantum gases, Nat. Phys. **8**, 267 (2012).
[2] R. Blatt and C. F. Roos, Quantum simulations with trapped ions, Nat. Phys. **8**, 277 (2012).
[3] C. W. Bauer, Z. Davoudi, A. B. Balantekin, T. Bhattacharya, M. Carena, W. A. de Jong, P. Draper, A. El-Khadra, N. Gemelke, M. Hanada *et al.*, Quantum simulation for high-energy physics, PRX Quantum **4**, 027001 (2023).
[4] E. Poli, T. Bland, S. J. M. White, M. J. Mark, F. Ferlaino, S. Trabucco, and M. Mannarelli, Glitches in rotating supersolids, Phys. Rev. Lett. **131**, 223401 (2023).
[5] V. Amitrano, A. Roggero, P. Luchi, F. Turro, L. Vespucci, and F. Pederiva, Trapped-ion quantum simulation of collective neutrino oscillations, Phys. Rev. D **107**, 023007 (2023).
[6] J. Feldmann, K. Leo, J. Shah, D. A. B. Miller, J. E. Cunningham, T. Meier, G. von Plessen, A. Schulze, P. Thomas,

and S. Schmitt-Rink, Optical investigation of Bloch oscillations in a semiconductor superlattice, Phys. Rev. B **46**, 7252 (1992).

[7] O. Morsch, J. H. Müller, M. Cristiani, D. Ciampini, and E. Arimondo, Bloch oscillations and mean-field effects of Bose-Einstein condensates in 1D optical lattices, Phys. Rev. Lett. **87**, 140402 (2001).

[8] M. Drewsen, Ion Coulomb crystals, Physica B **460**, 105 (2015).

[9] D. J. Wineland, J. C. Bergquist, W. M. Itano, J. J. Bollinger, and C. H. Manney, Atomic-ion Coulomb clusters in an ion trap, Phys. Rev. Lett. **59**, 2935 (1987).

[10] L. Duca, N. Mizukami, E. Perego, M. Inguscio, and C. Sias, Orientational melting in a mesoscopic system of charged particles, Phys. Rev. Lett. **131**, 083602 (2023).

[11] E. Urban, N. Glikin, S. Mouradian, K. Krimmel, B. Hemmerling, and H. Haeffner, Coherent control of the rotational degree of freedom of a two-ion Coulomb crystal, Phys. Rev. Lett. **123**, 133202 (2019).

[12] G. Morigi, J. Bollinger, M. Drewsen, D. Podolsky, and E. Shimshoni, Ion Coulomb crystals: An exotic form of condensed matter, Rev. Mod. Phys. **98**, 035001 (2026).

[13] J. B. M. M. H. Landa, B. Reznik and T. Schaetz, Structure, dynamics and bifurcations of discrete solitons in trapped ion crystals, New J. Phys. **15**, 093003 (2013).

[14] I. Waki, S. Kassner, G. Birkl, and H. Walther, Observation of ordered structures of laser-cooled ions in a quadrupole storage ring, Phys. Rev. Lett. **68**, 2007 (1992).

[15] G. Birkl, S. Kassner, and H. Walther, Multiple-shell structures of laser-cooled $^{24}Mg^{+}$ ions in a quadrupole storage ring, Nature (London) **357**, 310 (1992).

[16] C. Schneider, D. Porras, and T. Schaetz, Experimental quantum simulations of many-body physics with trapped ions, Rep. Prog. Phys. **75**, 024401 (2012).

[17] S. Mavadia, J. F. Goodwin, G. Stutter, S. Bharadia, D. R. Crick, D. M. Segal, and R. C. Thompson, Control of the conformations of ion Coulomb crystals in a Penning trap, Nat. Commun. **4**, 2571 (2013).

[18] S. Fishman, G. De Chiara, T. Calarco, and G. Morigi, Structural phase transitions in low-dimensional ion crystals, Phys. Rev. B **77**, 064111 (2008).

[19] J. Kiethe, L. Timm, H. Landa, D. Kalincev, G. Morigi, and T. E. Mehlstäubler, Finite-temperature spectrum at the symmetry-breaking linear to zigzag transition, Phys. Rev. B **103**, 104106 (2021).

[20] S. Ulm, J. Roßnagel, G. Jacob, C. Degünther, S. T. Dawkins, U. G. Poschinger, R. Nigmatullin, A. Retzker, M. B. Plenio, F. Schmidt-Kaler, and K. Singer, Observation of the Kibble–Zurek scaling law for defect formation in ion crystals, Nat. Commun. **4**, 2290 (2013).

[21] A. Retzker, R. C. Thompson, D. M. Segal, and M. B. Plenio, Double well potentials and quantum phase transitions in ion traps, Phys. Rev. Lett. **101**, 260504 (2008).

[22] A. Choudhury, J. A. DeVine, S. Sinha, J. A. Lau, A. Kandratsenka, D. Schwarzer, P. Saalfrank, and A. M. Wodtke, Condensed-phase isomerization through tunnelling gateways, Nature (London) **612**, 691 (2022).

[23] G. Vogt, G. Krampert, P. Niklaus, P. Nuernberger, and G. Gerber, Optimal control of photoisomerization, Phys. Rev. Lett. **94**, 068305 (2005).

[24] M. Kübel, M. Spanner, Z. Dube, A. Y. Naumov, S. Chelkowski, A. D. Bandrauk, M. J. J. Vrakking, P. B. Corkum, D. M. Villeneuve, and A. Staudte, Probing multiphoton light-induced molecular potentials, Nat. Commun. **11**, 2596 (2020).

[25] T. Stauch and A. Dreuw, Advances in quantum mechanochemistry: Electronic structure methods and force analysis, Chem. Rev. **116**, 14137 (2016).

[26] A. C. Aragonès, N. L. Haworth, N. Darwish, S. Ciampi, E. J. Mannix, G. G. Wallace, I. Diez-Perez, and M. L. Coote, Electrostatic catalysis of a Diels–Alder reaction, Nature (London) **531**, 88 (2016).

[27] D. R. Widmer and B. J. Schwartz, Solvents can control solute molecular identity, Nat. Chem. **10**, 910 (2018).

[28] L. L. Yan, W. Wan, L. Chen, F. Zhou, S. J. Gong, X. Tong, and M. Feng, Exploring structural phase transitions of ion crystals, Sci. Rep. **6**, 21547 (2016).

[29] A. Ayyadevara, A. Prakash, S. Dutta, A. Paramekanti, and S. A. Rangwala, Observing octupolar charge orders and their transition dynamics in Coulomb clusters, Phys. Rev. Res. **8**, L012066 (2026).

[30] A. Noguchi, Y. Shikano, K. Toyoda, and S. Urabe, Aharonov–Bohm effect in the tunnelling of a quantum rotor in a linear Paul trap, Nat. Commun. **5**, 3868 (2014).

[31] M. Mallweger, N. Kuk, V. Shankar, R. Thomm, H. Parke, I. Straka, W. Li, I. Lesanovsky, and M. Hennrich, Electronic state-dependent conformational changes in a Rydberg ion crystal, Phys. Rev. Lett. **137**, 063602 (2026).

[32] D. H. E. Dubin, Theory of structural phase transitions in a trapped Coulomb crystal, Phys. Rev. Lett. **71**, 2753 (1993).

[33] T. B. Mitchell, J. J. Bollinger, D. H. E. Dubin, X.-P. Huang, W. M. Itano, and R. H. Baughman, Direct observations of structural phase transitions in planar crystallized ion plasmas, Science **282**, 1290 (1998).

[34] D. Kiesenhofer, H. Hainzer, A. Zhdanov, P. C. Holz, M. Bock, T. Ollikainen, and C. F. Roos, Controlling two-dimensional Coulomb crystals of more than 100 ions in a monolithic radio-frequency trap, PRX Quantum **4**, 020317 (2023).

[35] E. Perego, L. Duca, and C. Sias, Electro-optical ion trap for experiments with atom-ion quantum hybrid systems, Appl. Sci. **10**, 2222 (2020).

[36] K. Pyka, J. Keller, H. L. Partner, R. Nigmatullin, T. Burgermeister, D. M. Meier, K. Kuhlmann, A. Retzker, M. B. Plenio, W. H. Zurek, A. del Campo, and T. E. Mehlstäubler, Topological defect formation and spontaneous symmetry breaking in ion Coulomb crystals, Nat. Commun. **4**, 2291 (2013).

[37] M. Kong, B. Partoens, and F. M. Peeters, Transition between ground state and metastable states in classical two-dimensional atoms, Phys. Rev. E **65**, 046602 (2002).

[38] M. Marlo, M. Alatalo, A. Harju, and R. M. Nieminen, Lateral diatomic two-dimensional artificial molecules: Classical transitions and quantum-mechanical counterparts, Phys. Rev. B **66**, 155322 (2002).

[39] P. Hänggi, P. Talkner, and M. Borkovec, Reaction-rate theory: Fifty years after Kramers, Rev. Mod. Phys. **62**, 251 (1990).

[40] J. Brox, P. Kiefer, M. Bujak, T. Schaetz, and H. Landa, Spectroscopy and directed transport of topological solitons

in crystals of trapped ions, Phys. Rev. Lett. **119**, 153602 (2017).

[41] P. Horak, A. Dantan, and M. Drewsen, Optically induced structural phase transitions in ion Coulomb crystals, Phys. Rev. A **86**, 043435 (2012).

[42] M. Mielenz, H. Kalis, M. Wittemer, F. Hakelberg, U. Warring, R. Schmied, M. Blain, P. Maunz, D. L. Moehring, D. Leibfried, and T. Schaetz, Arrays of individually controlled ions suitable for two-dimensional quantum simulations, Nat. Commun. **7**, ncomms11839 (2016).

[43] S.-A. Guo, Y.-K. Wu, J. Ye, L. Zhang, W.-Q. Lian, R. Yao, Y. Wang, R.-Y. Yan, Y.-J. Yi, Y.-L. Xu, B.-W. Li, Y.-H. Hou, Y.-Z. Xu, W.-X. Guo, C. Zhang, B.-X. Qi, Z.-C. Zhou, L. He, and L.-M. Duan, A site-resolved two-dimensional quantum simulator with hundreds of trapped ions, Nature (London) **630**, 613 (2024).

[44] M. K. Joshi, P. Hrmo, V. Jarlaud, F. Oehl, and R. C. Thompson, Population dynamics in sideband cooling of trapped ions outside the Lamb-Dicke regime, Phys. Rev. A **99**, 013423 (2019).

[45] F. Thielemann, J. Siemund, D. von Schoenfeld, W. Wu, P. Weckesser, K. Jachymski, T. Walker, and T. Schaetz, Exploring atom-ion Feshbach resonances below the *s*-wave limit, Phys. Rev. X **15**, 011051 (2025).

[46] C. Sias, Emulating isomerization with two-dimensional Coulomb crystals [Dataset], Zenodo, 2025, https://doi.org/10.5281/zenodo.17341417.